Available online at www.sciencedirect.com

ScienceDirect

Ceramics International 40 (2014) 93–99

CERAMICS INTERNATIONAL

www.elsevier.com/locate/ceramint

Preparation and performance of MAO coatings obtained on AZ91D Mg alloy under unipolar and bipolar modes in a novel dual electrolyte

Shuyan Wang[a,b,*], Yongping Xia[b], Li Liu[b], Naichao Si[a]

[a]School of Material Science and Engineering, Jiangsu University, Zhenjiang 212013, China
[b]School of Materials Science and Engineering, Jiangsu University of Science and Technology, Zhenjiang 212003, China

Received 20 February 2013; received in revised form 26 May 2013; accepted 28 May 2013
Available online 4 June 2013

Abstract

Ceramic coatings were obtained on AZ91D magnesium alloy by microarc oxidation under unipolar and bipolar modes in a silicate–aluminate dual electrolyte. The surface and cross-sectional morphology, coating thickness and phase composition of coatings were characterized by scanning electron microscopy (SEM), layer thickness meter and X-ray diffraction (XRD), respectively. The corrosion resistance of coatings in a 3.5% NaCl neutral solution was evaluated by electrochemical impedance spectroscopy (EIS) and potentiodynamic polarization. The results showed that the microarc oxidation (MAO) process in the unipolar mode was very similar to that in the bipolar mode. The average thickness of the coating obtained in the unipolar mode was thinner than that in the bipolar mode. Both coatings were mainly composed of MgO, Mg_2SiO_4 and $MgAl_2O_4$. Introduction of a cathodic component during the MAO process was helpful to obtain a uniform and compact coating. The electrochemical study indicated that the coating obtained in the bipolar mode was in better corrosion resistance due to its compact microstructure and thickness.

Keywords: Magnesium alloy; Microarc oxidation; Unipolar; Dual electrolyte; Corrosion resistance

1. Introduction

Magnesium alloy is the lightest structural metallic material, which is widely used in many industries such as aerospace, automobile and communication fields because of its high strengh to weight ratio, good cast ability, good electromagnetic shielding, high dimensional stability and recycling ability [1,2]. However, magnesium alloys exhibit a high chemical activity, so the corrosion resistance of magnesium alloys is poor which restricts its wide application in many situations [3]. Therefore, some surface modification techniques have been applied to improve the corrosion resistance, including electrochemical plating conversion coating [4], chemical conversion coating [5], anodzing [6], laser surface melting [7], organic coating [8], etc. Recently, MAO as a new surface modification has been brought to produce ceramic coatings on many metals such as Mg, Al, Ti and its alloys [9–12]. The corrosion and wear resistance can be remarkably improved after the MAO process [13,14].

The charactersitics of MAO coatings are determined not only by the nature of substrate and the electrolyte, but also by the applied electrical parameters and type of power source. In recent studies, many power sources such as DC, AC and pulsed bipolar power sources are used to produce MAO coatings [15,16]. It is established that AC, pulsed DC and bipolar power sources can be used to produce a more uniform and less porous coating as compared to DC sources [17]. Gnedenkov has analyzed MAO coatings obtained on an Mg–Mn type alloy under unipolar and bipolar constant voltage modes in a single electrolyte system [18], but a systematic study about the effects of MAO mode on the MAO process and characteristics of coatings in a dual electrolyte system has not been well documented in literatures. Therefore, in present work, an opimized dual electrolyte system consisting of

*Corresponding author at: School of Material Science and Engineering, Jiangsu University, Zhenjiang 212013, China. Tel./fax: +86 511 8442 6291.
E-mail address: wsy101010@126.com (S. Wang).

0272-8842/$ - see front matter
http://dx.doi.org/10.1016/j.ceramint.2013.05.108

silicate (Na_2SiO_3) and aluminate ($NaAlO_2$) as well as the additives of $Na_2B_4O_7$, NaOH, $C_3H_8O_3$ and $C_6H_5Na_3O_7$ was empolyed to produce MAO coatings under unipolar and bipolar constant current modes. In addition, the effects of MAO mode on MAO process, thickness, microstructure, phase composition and corrosion resistance of coatings were investigated.

2. Experimental

Rectangular samples ($15 \times 15 \times 5$ mm^3) of AZ91D magnesium alloy (8.91 wt% Al, 0.54 wt% Zn, 0.23 wt% Mn, 0.034 wt% Si, 0.0014 wt% Fe, and Mg balance) were used as substrates in the experiment. Prior to MAO process, samples were grounded with a series of silicon carbide waterproof abrasive papers (up to 2000 grits), and then ultrasonically washed in ethanol and distilled water.

MAO process was carried out using a WHD-20 MAO system with a pulsed bipolar AC power supply, a stainless steel bath used as the counter electrode and a stirring and cooling system keeping the temperature of the electrolyte below 40 °C. The dual electrolyte was prepared from distilled water, containing 15 g/L Na_2SiO_3, 9 g/L $NaAlO_2$, 2 g/L $Na_2B_4O_7$, 3 g/L NaOH, 5 ml/L $C_3H_8O_3$ and 7 g/L $C_6H_5Na_3O_7$. In the bipolar mode, the duty cycle was dominated by pulse width, namely, the positive and negative duty cycles were fixed at 38% and 30%, respectively. Similarly, the coating formation process in the unipolar mode was controlled by the number of pulses, and the quantity ratio of positive pulse to negative pulse was 1:0. Details of other parameters used in the MAO process are given in Table 1.

The thickness of coatings was evaluated by a layer thickness meter (CMI233). A scanning electron microscope (JSM-6480) was employed to analyze the surface and cross-sectional morphologies of coatings. X-ray diffraction (XRD-6000) operating with Cu K_α radiation was used to determine the phase composition of coatings. Electrochemical impedance spectroscopy (EIS) and potentiodynamic polarization were performed using the M283 electrochemical measurement system containing a potentiostat and a lock-in amplifier in a 3.5% NaCl neutral solution at room temperature. The EIS measurements were made at open circuit potential (OCP) with AC amplitude of 10 mV and a frequency ranged from 10^5 Hz to 10^{-2} Hz. The potentiodynamic polarization was carried out with a scanning rate of 1 mV/s and a scanning range from −250 mV vs. OCP to +250 mV vs. OCP. Prior to tests, coatings were immersed in a 3.5% NaCl neutral solution for 30 min to reach a stable potential. All electrochemical measurements were performed with a conventional three-electrode cell consisting of a platinum electrode as the counter electrode, a saturated calomel electrode as the reference electrode and MAO coatings as the working electrode.

3. Results and discussion

3.1. Voltage–time response

Fig. 1 shows the dependence of voltage on the oxidation time obtained in different modes. It can be concluded that all the MAO processes can be divided into three distinguishing stages according to the increasing rate of voltage and variation of sparks. The variation of voltage in three different stages viz.:(i) general anodization, (ii) rapid growth of the coating and (iii) local growth of the coating, is presented in Table 2. MAO modes have no effect on the striking voltage, and sparks began to be observed at around 202 V both in the unipolar and bipolar modes. In the bipolar mode, the voltage increased linearly with time at a slope of 4.39 V/s in the stage I (0–46 s), and a slightly thin dielectric film began to form on the surface of the magnesium alloy, resulting in the rapid rising of voltage [19], meanwhile, no sparks can be seen in the first stage. With the extension of time, the voltage continually increased from 202 V to 386 V, however, the increasing rate of voltage decreased to 0.93 V/s in stage II(46–243 s), and a lot of silvery white moving sparks with small size were distributed evenly on the surface of samples during the whole MAO process. After stage II, the voltage–time response slope dropped rapidly (0.08 V/s) and the voltage reached a final value of 441 V. In stage III, white sparks changed to numerous separate orange ones with big size. In the unipolar mode, the trend about the

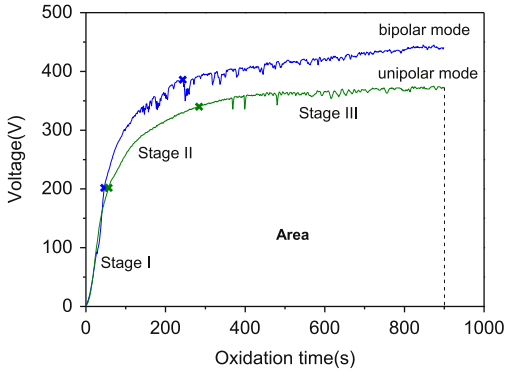

Fig. 1. Variations of voltage with time during MAO process in the unipolar and bipolar modes.

Table 1
Other parameters used in the MAO process.

Sample	Anodic current density (A dm^{-2})	Cathodic current density (A dm^{-2})	Frequency (Hz)	Treating time (min)
Bipolar mode	15	18	520	15
Unipolar mode	15	0		

Table 2
Stages of MAO process in the unipolar and bipolar modes.

Sample	Stage I	Stage II	Stage III
Bipolar mode	Up to ~202 V (0–46 s)	202–386 V (46–243 s)	386–441 V (243–900 s)
Unipolar mode	Up to ~202 V (0–57 s)	202–340 V (57–284 s)	340–373 V (284–900 s)

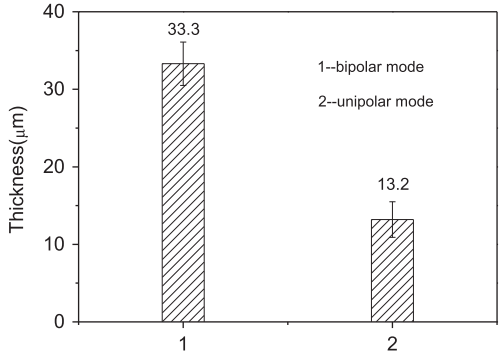

Fig. 2. Thickness of MAO coatings obtained in the unipolar and bipolar modes.

increasing rate of voltage was similar to that in the bipolar mode, namely, with the extension of time, the increasing rate of voltage decreased gradually. In addition, the final voltage in the unipolar mode decreased 68 V compared to the bipolar one, and the time when the voltage increased to the striking voltage was slightly longer in the unipolar mode. Moreover, the size of sparks in stage III observed in the unipolar mode was larger than that in the bipolar mode, and the buzzing at the end of MAO process in the unipolar mode was louder than that in the bipolar mode, which may be caused by a more drastic reaction.

3.2. Thickness and morphology

Fig. 2 demonstrates the thickness of MAO coatings obtained in the unipolar and bipolar modes. It can be seen that the coating obtained in the bipolar mode was about 33.3 μm, whereas it was much thinner which was about 13.2 μm in the unipolar mode. In the constant current mode, the total energy consumption during the whole MAO process can be expressed as following equation [20]:

$$E = S\int_0^t U(t)jdt \quad (1)$$

where S is the area of a sample, j is the current density, and $U(t)$ is a variable vs. time. Because the area and current density of each sample were the same, the total energy consumption can be expressed using the area covered by each voltage–time curve (shown in Fig. 1). The bigger the area was, the larger the total energy consumption was, which indicated that the growth rate of coatings was higher. As shown in Fig. 1, the area in the bipolar mode was larger than that in the unipolar mode, thus, with the same treating time, the coating obtained in the bipolar mode was thicker.

Fig. 3 represents the surface and cross-sectional morphologies of MAO coatings prepared in different modes. It was found that mophologies of MAO coatings were influenced remarkably by the MAO mode. As seen in Fig. 3(a,b), MAO coatings presented a sintered microstructure with some pores and microcracks distributed disorderly on the surface of coatings. In the unipolar mode, the number of pores seemed to decrease, however, the coating was very rough and the size of ceramic particles distributed on the surface was also quite large. As known, the size of sparks during the whole MAO process has great influence on the ultimate morphology of coatings. Because the size of sparks observed in the unipolar mode was larger than that in the bipolar mode, the reaction was more drastic during the formation of coatings in the unipolar mode, thus, some pores may be covered by molten oxides at the end of MAO process. In Fig. 3(c,d), the coating obtained in the unipolar mode was not uniform compared to that in the bipolar mode, and many pores with bigger size existed in the coating. Moreover, the coating obtained in the bipolar mode was relatively uniform and compact, and there were only a spot of small pores and microcracks, however, these defects did not penetrate through the whole coating.

3.3. Phase composition

X-ray diffraction patterns of AZ91D magnesium alloy and MAO coatings obtained in the unipolar and bipolar modes are shown in Fig. 4. It was found that both MAO coatings were composed of MgO, Mg_2SiO_4 and $MgAl_2O_4$, indicating that both the magnesium alloy and the elctrolyte componment were involved in the formation of MAO coatings. The presence of Mg peaks was caused by the substrate, suggesting that X-ray can easily penetrate through the coating and reach the substrate. As shown in Fig. 4, the intensity of Mg peaks in the pattern of the coating in the bipolar mode was weaker compared to that in the unipolar mode, because the coating in the bipolar mode was thicker and more compact.

Yerokhin [21] reported that complex-ion $[Al(OH)_4]^-$ or $[Al_n(OH)_{4n+2}]^{(n+2)-}$ existed in the electrolyte instead of AlO_2^- anion. During the MAO process, magnesium alloy was dissolved and a lot of Mg^{2+} was absorbed on the surface of the sample, meanwhile, SiO_3^{2-}, OH^-, $[Al(OH)_4]^-$ and $[Al_n(OH)_{4n+2}]^{(n+2)-}$ negative ions were pushed forward toward the sample by the force of electric field. Consequently, the presence of Mg_2SiO_4 was due to a chemical reaction occurring among SiO_3^{2-}, OH^- and Mg^{2+}, as described in the literatures [22].

$$Mg - 2e \rightarrow Mg^{2+} \quad (2)$$

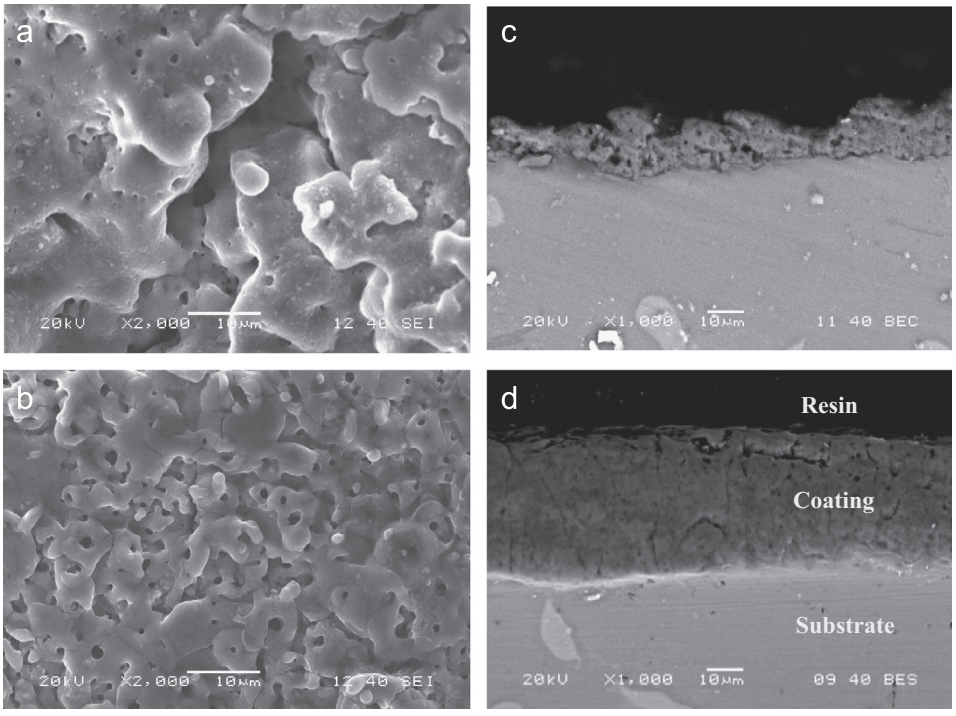

Fig. 3. Surface and cross-sectional morphology of MAO coatings fabricated on AZ91D magnesium alloy (a,c) in the unipolar mode and (b,d) in the bipolar mode.

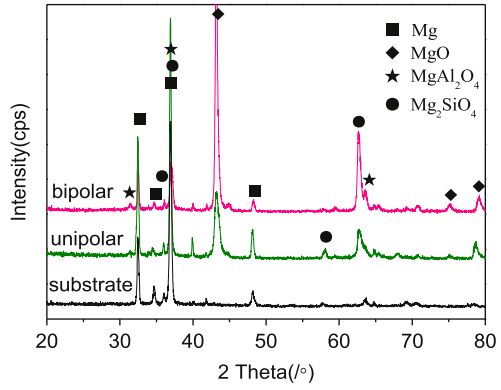

Fig. 4. XRD patterns of substrate and MAO coatings obtained in the unipolar and bipolar modes.

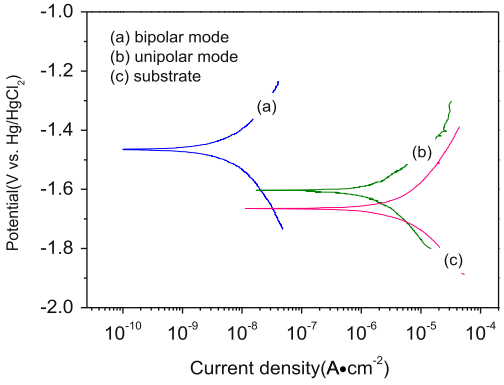

Fig. 5. Potentiodynamic polarization curves of substrate and coatings obtained under different MAO modes in a 3.5 wt% NaCl neutral solution.

$$2Mg^{2+} + SiO_3^{2-} + 2OH^- \rightarrow Mg_2SiO_4 + H_2O \quad (3)$$

The formation of MgO phase was due to the dehydration of $Mg(OH)_2$ as a result of the high temperature during the sparking discharge process [23]. The presence of $MgAl_2O_4$ phase was attributed to the reaction between Mg^{2+} and $[Al(OH)_4]^-$ or $[Al_n(OH)_{4n+2}]^{(n+2)-}$.

$$Mg^{2+} + 2OH^- \rightarrow Mg(OH)_2 \rightarrow MgO + H_2O \quad (4)$$

$$Mg^{2+} + 2[Al(OH)_4]^- \rightarrow MgAl_2O_4 + 4H_2O \quad (5)$$

$$(n+2)Mg^2 + 2[Al_n(OH)_{4n+2}]^{(n+2)-} \rightarrow nMgAl_2O_4 + 2Mg(OH)_2 + 4nH_2O \quad (6)$$

3.4. Electrochemical study

3.4.1. Potentiodynamic polarization

Fig. 5 demonstrates the polarization curves of AZ91D magnesium alloy and MAO coatings obtained in different MAO modes. The anodic/cathodic Tafel slopes, corrosion potential and corrosion current density were derived by a software named corrview. The vaules of polarization resistance (R_p) were determined by the Stern–Geary equation according to the approximately linear polarization behavior near OCP [24]

$$R_p = \frac{b_a b_c}{2.303 i_{corr}(b_a + b_c)} \quad (7)$$

All the electrochemical data derived from potentiodynamic polarization curves in Fig. 5 are listed in Table 3. A higher

Table 3
Fitting data for the bare alloy and MAO coatings from potentiodynamic polarization curves.

Specimen	b_a (mV)	b_c (mV)	E_{corr} (V vs. Hg/HgCl$_2$)	i_{corr} (A/cm^2)	R_p (Ω cm^2)
Substrate	303.31	231.33	−1.6654	6.7902×10^{-6}	8.3923×10^{3}
Bipolar mode	330.29	334.95	−1.4651	9.6821×10^{-9}	7.4582×10^{6}
Unipolar mode	156.17	200.76	−1.6026	1.5956×10^{-6}	2.3904×10^{4}

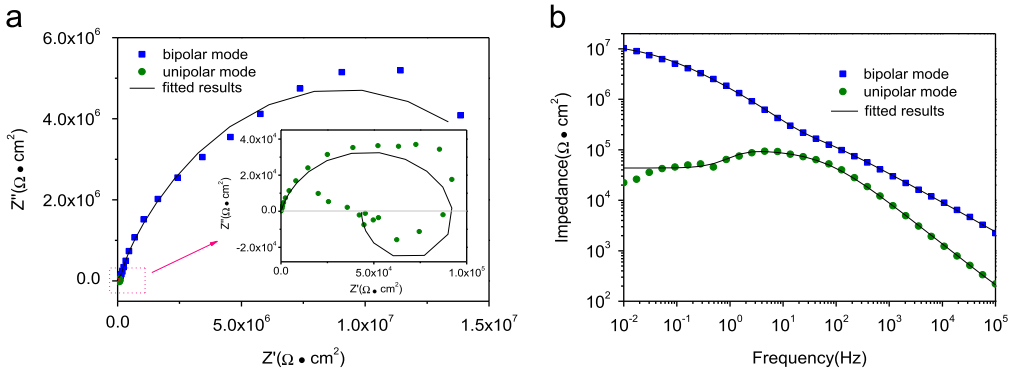

Fig. 6. Experimental and fitting (a) Nyquist and (b) Bode plots of MAO coatings formed in different MAO modes after 0.5 h of immersion in 3.5% NaCl neutral solution.

corrosion potential and polarization resistance as well as a lower corrosion current density demonstrates that it exhibits a good corrosion resistance. Similarly, it was evident that the coated sample exhibited a more positive corrosion potential and a larger vaule of polarization resistance as well as a lower corrosion current density as compared to the magnesium alloy, which indicated that the corrosion resistance of the magnesium alloy was significantly enhanced after the MAO process. In addition, it can be concluded that the coating obtained in the bipolar mode performed a better corrosion resistance than that in the unipolar mode. Compared with the substrate, the corrosion potential of the coating prepared in the bipolar mode increased nearly by 200 mV, while the corrosion current density decreased more than two orders of magnitude. Meanwhile, the polarization resistance increased nearly three orders of magnitude compared to the substrate. Generally, the corrosion resistance are determined by coating thickness, microstructure and chemical composition, etc [25,26]. As shown in Fig. 3, the coating obtained in the unipolar mode was very thin and loose, so the corrosive medium (e.g. Cl^-) was easier to move to the substrate through these microscopic defects, resulting in the coating with a poor corrosion resistance. On the contrary, the coating obtained in the bipolar mode was thick enough and its microstructure was relatively uniform and compact in the cross-section, so the coating exhibited a better corrosion reistance.

3.4.2. Electrochemical impedance spectroscopy

The EIS characteristics of coatings obtained in different MAO modes are shown in Fig. 6. The radius of the capacitive loop respresents the corrosion resistance of coatings. As seen in Fig. 6a, the coating obtained in the bipolar mode exhibited a larger capacitive loop, indicating that it provided a more effective corrosion resistance protection as compared to that

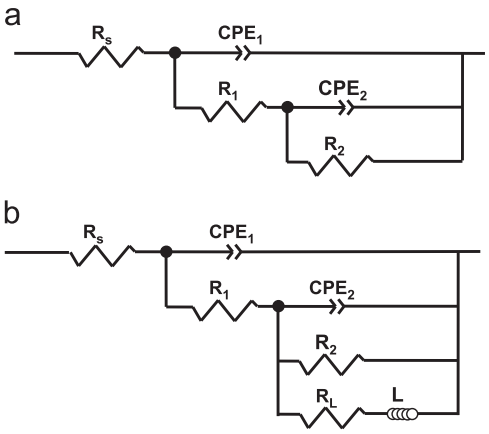

Fig. 7. Equivalent circuits for fitting the impedance data of MAO coatings.

formed in the unipolar mode. The EIS results were consistent with those of potentiodynamic polarization. According to the characteristics of corrosive process in the electrochemical reaction system and some literatures [27,28], two widely accepted models employed for curve fitting of MAO coatings are illustrated in Fig. 7. The values of fitting circuit elements are listed in Table 4. In the equivalent circuits, R_s is the solution resistance, R_1 is the resistance of the outer loose layer paralleled with constant phase element CPE1, R_2 represents the resistance of the inner dense layer paralleled with CPE2, and R_L is the charge transfer resistance of pitting corrosion in series with the inductance L. Constant phase elements (CPE) were used in the electrochemical circuit instead of capacitors in order to account for the surface heterogeneity and diffusion factors, and the admittance of CPE is expressed as [29]

$$Z_{CPE} = \frac{1}{T(j\omega)^n} \quad (8)$$

Table 4
Fitting results of EIS plots of MAO coatings under different MAO modes after 0.5 h of immersion in a 3.5% NaCl neutral solution.

Specimen	$(CPE\text{-}T)_1$ ($S\ cm^{-2}\ s^{-n}$)	n_1	R_1 ($\Omega\ cm^2$)	$(CPE\text{-}T)_2$ ($S\ cm^{-2}\ s^{-n}$)	n_2	R_2 ($\Omega\ cm^2$)	L (H)	R_L ($\Omega\ cm^2$)
Bipolar mode	8.828×10^{-8}	0.4176	5.128×10^5	6.826×10^{-9}	0.7143	1.279×10^7	—	—
Unipolar mode	7.446×10^{-7}	0.8339	3.713×10^4	6.071×10^{-6}	0.8	1.387×10^5	7460	6866

where T is the CPE constant, j is the imaginary unit, ω is the angular frequency and n is the CPE exponent. Depending on the value of n, CPE can represent resistance when $n=0$, capacitance when $n=1$ and Warburg impedance when $n=0.5$.

It was obvious from Fig. 6 that MAO coatings obtained in different modes had different corrosion charactersitcs. In Fig. 6a, the appearance of inductive loop in the coating obtained in the unipolar mode indicated that the corrosive medium (e.g. Cl^-) had already induced the corrosion of the substrate, which proved that the coating did not protect the substrate from corrosion effectively. As shown in Table 4, the coating obtained in the unipolar mode had a lower resistance R_1 and R_2 as compared to those in the bipolar mode. The cross-sectional morphologies of coatings in Fig. 3 clearly reveal that the coating obtained in the bipolar mode is more compact than that in the unipolar mode. The seepage of electrolyte into the substrate through the defects (shown in Fig. 3c) is responsible for its poor corrosion resistance. In addidtion, the value of R_2 is always higher than R_1 of the coating obtained in different MAO modes, indicating that the outer loose layer was not able to provide a high resistance against the corrosion and the corrosion resistance of the coating was mainly detemined by the inner dense layer.

4. Conclusions

(1) The MAO process was similar both in the unipolar mode and bipolar mode. The average thickness of the coating obtained in the bipolar mode is about 33.3 μm, thicker than that obtained in the unipolar mode.
(2) Both coatings are mainly composed of MgO, Mg_2SiO_4 and $MgAl_2O_4$ phase. Introduction of a cathodic component during the MAO process is helpful to obtain a uniform and compact coating.
(3) Based on the results of EIS and potentiodynamic polarization, the coating obtained in the bipolar mode demonstrates a more effective protection for the magnesium alloy due to its compact microstructure and thickness.

Acknowledgments

This work was financially supported by a project funded by the Priority Academic Program Development of Jiangsu Higher Education Institutions under Grant (No. 12504230006).

References

[1] P.D. Caton, Magnesium-an old material with new applications, Materials and Design 12 (1991) 309–316.
[2] B.L. Mordike, T. Ebert, Magnesium: properties-applications-potential, Materials Science and Engineering: A 302 (2001) 37–45.
[3] J.E. Gray, B. Luan, Protective coatings on magnesium and its alloys-a critical review, Journal of Alloys and Compounds 336 (2002) 88–113.
[4] WU Li-ping, ZHAO Jing-jing, XIE Yong-ping, YANG Zhong-dong, Progress of electroplating and electroless plating on magnesium alloy, Transactions of Nonferrous Metals Society of China 20 (2010) s630–s637.
[5] K.H. Yang, M.D. Ger, W.H. Hwu, Y. Sung, Y.C. Liu, Study of vanadium-based chemical conversion coating on the corrosion resistance of magnesium alloy, Materials Chemistry and Physics 101 (2007) 480–485.
[6] Yan Liu, Zhongling Wei, Fuwei Yang, Zhao Zhang, Environmental friendly anodizing of AZ91D magnesium alloy in alkaline borate–benzoate electrolyte, Journal of Alloys and Compounds 509 (2011) 6440–6446.
[7] J. Dutta Majumdar, R. Galun, B.L. Mordike, I. Manna, Effect of laser surface melting on corrosion and wear resistance of a commercial magnesium alloy, Materials Science and Engineering: A 361 (2003) 119–129.
[8] Rong-Gang Hu, Su Zhang, Jun-Fu Bu, Chang-Jian Lin, Guang-Ling Song, Recent progress in corrosion protection of magnesium alloys by organic coatings, Progress in Organic Coatings 73 (2012) 129–141.
[9] P. Shi, W.F. Ng, M.H. Wong, F.T. Cheng, Improvement of corrosion resistance of pure magnesium in Hanks' solution by microarc oxidation with sol–gel TiO_2 sealing, Journal of Alloys and Compounds 469 (2009) 286–292.
[10] Lei Wen, Yaming Wang, Yu Zhou, Lixin Guo, Jia-Hu Ouyang, Microstructure and corrosion resistance of modified 2024 Al alloy using surface mechanical attrition treatment combined with microarc oxidation process, Corrosion Science 53 (2011) 473–480.
[11] Yaming Wang, Tingquan Lei, Bailing Jiang, Lixin Guo, Growth, microstructure and mechanical properties of microarc oxidation coatings on titanium alloy in phosphate-containing solution, Applied Surface Science 233 (2004) 258–267.
[12] Emrah Cakmak, Kadir Tekin, Ugur Malayoglu, Suman Shrestha, The effect of substrate composition on the electrochemical and mechanical properties of PEO coatings on Mg alloys, Surface and Coatings Technology 204 (2010) 1305–1313.
[13] J. Liang, P. Bala Srinivasan, C. Blawert, W. Dietzel, Comparison of electrochemical corrosion behaviour of MgO and ZrO_2 coatings on AM50 magnesium alloy formed by plasma electrolytic oxidation, Corrosion Science 51 (2009) 2483–2492.
[14] P. Bala Srinivasan, C. Blawert, W. Dietzel, Dry sliding wear behaviour of plasma electrolytic oxidation coated AZ91 cast magnesium alloy, Wear 266 (2009) 1241–1247.
[15] Chang Lin-rong, Cao Fa-he, Cai Jing-shun, Liu Wen-juan, Zhang Zhao, Zhang Jian-qing, Influence of electric parameters on MAO of AZ91D magnesium alloy using alternative square-wave power source, Transactions of Nonferrous Metals Society of China 21 (2011) 307–316.
[16] A.L. Yerokhin, X. Nie, A. Leyland, A. Matthews, S.J. Dowey, Plasma electrolysis for surface engineering, Surface and Coatings Technology 122 (1999) 73–93.
[17] Shigang Xin, Lixin Song, Ronggen Zhao, Xingfan Hu, Influence of cathodic current on composition, structure and properties of Al_2O_3 coatings on aluminum alloy prepared by micro-arc oxidation process, Thin Solid Films 515 (2006) 326–332.
[18] S.V. Gnedenkov, O.A. Khrisanfova, A.G. Zavidnaya, S.L. Sinebryukhov, V.S. Egorkin, M.V. Nistratova, A. Yerokhin, A. Matthews, PEO coatings

obtained on an Mg–Mn type alloy under unipolar and bipolar modes in silicate-containing electrolytes, Surface and Coatings Technology 204 (2010) 2316–2322.

[19] Liu Feng, Shan Da-yong, Song Ying-wei, Han En-hou, Formation process of composite plasma electrolytic oxidation coating containing zirconium oxides on AM50 magnesium alloy, Transactions of Nonferrous Metals Society of China 21 (2011) 943–948.

[20] H.B. Wang, Z.G. Fang, B.L. Jiang, in: Microarc Oxidation Technology and its Applications in Sea Environments, first ed., National Defense Industry Press, Beijing, 2010 (in Chinese).

[21] A.L. Yerokhin, A. Leyland, A. Matthews, Kinetic aspects of aluminium titanate layer formation on titanium alloys by plasma electrolytic oxidation, Applied Surface Science 200 (2002) 172–184.

[22] H.F. Guo, M.Z. An, H.B. Huo, S. Xu, L.J. Wu, Microstructure characteristic of ceramic coatings fabricated on magnesium alloys by micro-arc oxidation in alkaline silicate solutions, Applied Surface Science 252 (2006) 7911–7916.

[23] Y. Ma, X. Nie, D.O. Northwood, H. Hu, Systematic study of the electrolytic plasma oxidation process on a Mg alloy for corrosion protection, Thin Solid films 494 (2006) 296–301.

[24] M. Stern, A.L. Geary, A theoretical analysis of the shape of polarization curves, Journal of The Electrochemical Society 104 (1957) 56–63.

[25] Guo-Hua Lv, Huan Chen, Xing-Quan Wang, Hua Pang, Gu-Ling Zhang, Bin Zou, Heon-Ju Lee, Si-Ze Yang, Effect of additives on structure and corrosion resistance of plasma electrolytic oxidation coatings on AZ91D magnesium alloy in phosphate based electrolyte, Surface and Coatings Technology 205 (2010) S36–S40.

[26] Huan Chen, Guo-Hua Lv, Gu-Ling Zhang, Hua Pang, Xing-Quan Wang, Heon-Ju Lee, Si-Ze Yang, Corrosion performance of plasma electrolytic oxidized AZ31 magnesium alloy in silicate solutions with different additives, Surface and Coatings Technology 205 (2010) S32–S35.

[27] A. Ghasemi, V.S. Raja, C. Blawert, W. Dietzel, K.U. Kainer, The role of anions in the formation and corrosion resistance of the plasma electrolytic oxidation coatings, Surface and Coatings Technology 204 (2010) 1469–1478.

[28] J. Liang, P. Bala Srinivasan, C. Blawert, M. StÖrmer, W. Dietzel, Electrochemical corrosion behaviour of plasma electrolytic oxidation coatings on AM50 magnesium alloy formed in silicate and phosphate based electrolytes, Electrochimica Acta 54 (2009) 3842–3850.

[29] P. Bala Srinivasan, J. Liang, C. Blawert, M. StÖrmer, W. Dietzel, Effect of current density on the microstructure and corrosion behaviour of plasma electrolytic oxidation treated AM50 magnesium alloy, Applied Surface Science 255 (2009) 4212–4218.